Nano Research 2018, 11(6): 3154–3163
https://doi.org/10.1007/s12274-017-1690-4
Research Article
ISSN 1998-0124
CN 11-5974/O4

Investigation of black phosphorus as a nano-optical polarization element by polarized Raman spectroscopy

Nannan Mao[1], Shishu Zhang[1], Jinxiong Wu[1], Huihui Tian[1], Juanxia Wu[1], Hua Xu[2], Hailin Peng[1], Lianming Tong[1] (✉), and Jin Zhang[1] (✉)

[1] *Center for Nanochemistry, Beijing National Laboratory for Molecular Sciences, Key Laboratory for the Physics and Chemistry of Nanodevices, State Key Laboratory for Structural Chemistry of Unstable and Stable Species, College of Chemistry and Molecular Engineering, Peking University, Beijing 100871, China*

[2] *School of Materials Science and Engineering, Shaanxi Normal University, Xi'an 710062, China*

Received: 3 April 2017
Revised: 16 May 2017
Accepted: 19 May 2017

KEYWORDS
black phosphorus,
polarizing optics,
linear dichroism,
birefringence,
two-dimensional layered crystals

ABSTRACT

Manipulating the polarization of light at the nanoscale is essential for the development of nano-optical devices. Owing to its corrugated honeycomb structure, two-dimensional (2D) layered black phosphorus (BP) exhibits outstanding in-plane optical anisotropy with distinct linear dichroism and optical birefringence in the visible region, which are superior characteristics for ultrathin polarizing optics. Herein, taking advantage of polarized Raman spectroscopy, we demonstrate that layered BP with a nanometer thickness can remarkably alter the polarization state of a linearly-polarized laser and behave as an ultrathin optical polarization element in a BP-Bi_2Se_3 stacking structure by inducing the exceptionally polarized Raman scattering of isotropic Bi_2Se_3. Our findings provide a promising alternative for designing novel polarization optics based on 2D anisotropic materials, which can be easily integrated in micro-sized all-optical and optoelectronic devices.

1 Introduction

Integrated nano-optical and optoelectronic devices require effective approaches that allow modulating their responses to light at the nanoscale [1–4]. Recent advances along this line of research include the use of plasmonic nanostructures [3], resonators [5], and ultrathin dielectric materials [6, 7]. Owing to their remarkable photonic properties and two-dimensional (2D) nature, 2D layered crystals have attracted a great deal of interest for the development of miniaturized optical components, relying on their strong interaction with the light for the modulation of both phase and intensity [1, 8–12]. For instance, graphene has been successfully applied as a broadband transverse magnetic-pass and optically transparent microwave polarizer [9, 13]. On the other hand, transition metal dichalcogenides (TMDs) such as molybdenum disulfide

Address correspondence to Lianming Tong, tonglm@pku.edu.cn; Jin Zhang, jinzhang@pku.edu.cn

(MoS_2) have been demonstrated to possess polarization-selective absorption upon integration with optical waveguides, and have been used to prepare atomically thin optical lenses and gratings, due to their giant optical path length and elastic scattering efficiency [10, 12]. Since both graphene and MoS_2 are in-plane isotropic materials, polarizers based on these materials are mainly dependent on the different response to the light polarized parallel and perpendicular to the plane of the layered materials.

More recently, black phosphorus (BP), a layered material with a puckered structure and in-plane anisotropy, emerged among 2D materials [14–18]. Owing to their unique atomic corrugated layers, 2D BP crystals possess a distinctive in-plane optical anisotropic nature, which distinguishes them from graphene and many other analogues [14, 15, 19–26]. Thin BP layers exhibit strong anisotropic electron–photon and electron–phonon interactions, and previous studies have revealed that few-layer BP exhibits pronounced linear dichroism and birefringence features over a wide optical window, ranging from the visible to the near-infrared (NIR) light [21, 23, 24, 27–30]. Although the use of BP as a linear optical polarizer has been proposed before [27], previous investigations have been limited to the optical and optoelectronic responses of BP itself and its related p-n junction [31–34], such as broadband polarization-sensitive photodetectors [33]. Up to now, the capability of BP to change the light polarization by acting on a second material and modulating its optical response has not been effectively demonstrated.

Herein, we demonstrate that thin BP crystals with a 73-nm thickness can remarkably alter the polarization state of the incident light acting on Bi_2Se_3 crystals stacked with BP, leading to exceptionally polarized Raman signals of Bi_2Se_3. Under parallel polarization, all the Raman active modes of the Bi_2Se_3 crystal in the stacking structure exhibited their maximum and minimum intensities when the incident light was polarized along the zigzag (ZZ) and armchair (AC) directions of BP. The Raman intensity ratios between the maxima and minima were as high as 12 at 514.5 nm, suggesting a linear dichroism behavior of the thin BP layer in the stacking structure. Under cross polarization, the A_{1g} modes of the Bi_2Se_3 crystal, which should have been silent under cross polarization, not only appeared in the Raman spectrum of the BP-Bi_2Se_3 stacking structure, but also showed a clear polarization-angle dependence. This can be attributed to the pronounced modulation of the phase and amplitude of the incident polarized light induced by the combined effects of the linear dichroism and birefringence in the BP crystals, which were also explicitly supported by optical transmittance and reflection measurements under different polarization configurations. Our findings not only demonstrate that thin BP layers can serve as a polarizing optical element to manipulate the optical response of a Bi_2Se_3 sample, but also supply a convenient approach to prepare novel micro-optical elements based on 2D anisotropic crystals, which can be directly integrated into nanophotonic and optoelectronic devices.

2 Experimental

2.1 Sample preparation and characterization

Few-layer Bi_2Se_3 crystals were synthesized using the van der Waals epitaxy method on mica substrates. Thin BP samples were obtained by mechanical exfoliation from bulk BP crystals (Smart Elements). The BP-Bi_2Se_3 stacking structure was constructed by exfoliating the BP layers directly on the Bi_2Se_3 crystals deposited on the mica substrates. The optical images of the Bi_2Se_3 and BP flakes were obtained using an optical microscope (BX51), while their thicknesses were determined by atomic force microscopy (AFM, ICON).

2.2 Micro-transmittance measurements

Micro-transmittance measurements were conducted using the transmission mode of a WITec RSA300 optical microscope. Thin BP samples were exfoliated on a fused silica substrate. A halogen white light source KL 1500 (Zeiss) was used to illuminate the BP samples. The incident white light was focused on the surface of the BP flakes by a 100× objective lens. The transmitted light was collected by an inverted 60× objective lens and analyzed using a 300 mm focal length spectrometer with a standard FC/APC optical fiber entrance. An analyzer was placed in the light

collection path in front of the spectrometer, and the angle-resolved transmission was measured by rotating the polarization angle of the analyzer with an initial polarization angle of x direction. The transmittance (T) was calculated as $T = (I/I_0) \times 100\%$, where I and I_0 are the light intensities transmitted through the BP crystals and the nearby fused silica substrate, respectively.

2.3 Reflection spectra and Raman scattering spectra measurements

The reflection and Raman scattering measurements were carried out on a JY Horiba HR800 Raman system with a 100× objective lens and 600/mm grating. For the reflection measurements, a halogen lamp (EUROMEX, EK-1) was used as white light source, and the reflected signals were analyzed by a Raman spectrometer. The reflection spectra of BP were collected under cross polarization by rotating the BP samples, by adding one polarizer in the incident path and placing the analyzer in the collection path in front of the Raman spectrometer. The angle-dependent polarized Raman spectra of the BP and Bi_2Se_3 crystals were measured under both parallel and cross polarizations. Two different lasers (514.5 and 632.8 nm) were used to excite the Raman signals. The laser powers were kept lower than 100 μW to avoid laser-induced damages to the sample.

3 Results and discussion

As shown in Fig. 1(a), the BP crystals consist of a single element with the phosphorus atoms arranged in a puckering style. Since they belong to the orthorhombic crystal system, in principle the BP crystals possess different complex refractive indices along the three crystalline orientations i.e., x (zigzag, ZZ), y, and z (armchair, AC), thus exhibiting anisotropic absorption along the x and z axes, as well as the birefringence effect [14, 15, 23, 28], as illustrated in Figs. 1(a) and 1(d). Figures 1(b) and 1(e) show the polarized transmittance and reflection spectra of the thin BP flakes, respectively, obtained through mechanical exfoliation on a fused silica (Fig. 1(b)) and 300 nm SiO_2/Si (Fig. 1(e)) substrate. The transmittance spectra of the BP sample were measured using the transmission mode of a WITec RSA 300 system (Experimental section). The transmittance of BP was estimated as $T = (I/I_0) \times 100\%$ [33], where I and I_0 are the light intensities transmitted through the BP sample and the nearby blank fused silica substrate, respectively. Figure 1(b) illustrates the anisotropic transmittance spectra when the analyzer is polarized along the AC (blue curve) and ZZ (red curve) directions of the BP crystals in the pink region (65 nm thickness), respectively; the inset shows the optical image of this BP sample. Apparently, the BP sample transmits less and adsorbs more light polarized along the AC direction than the ZZ direction in the visible region, further confirming the linear dichroism in BP [14, 27]. It can also be seen that the transmittance difference along these two directions changes with the photon energy. To obtain further insight, we extracted the relative transmittance variation as a function of the rotation angle of the analyzer for this BP sample under the excitation wavelengths of 632.8 and 514.5 nm, respectively. As shown in Fig. 1(c), the BP sample exhibited its maximum absorption in correspondence of a sample rotation angle of 131° at both excitation wavelengths (the starting position is shown in the inset of Fig. 1(b)). Furthermore, the bowtie-shaped polar plot of BP's anisotropic transmittance at 514.5 nm was much thinner than that at 632.8 nm, indicating a stronger linear dichroism of the BP crystals at 514.5 nm [24], and thus a better performance when used as an absorptive linear polarizer. Under reflection mode, we observed that the thin BP sample showed an alternating brightness and darkness in the optical image upon cross polarization, when the sample was rotated at different angles (Fig. S1 in the Electronic Supplementary Material (ESM)). The sample became dark when the angle between the incident polarization and the straight edge was 0° and 90°, while it turned bright when the angle was 45° and 135°, consistent with earlier reports [28]. This directly indicates that the reflected light has a significant component of the polarization perpendicular to that of the incident light, which is a typical characteristic of the birefringence effect in BP crystals [19, 23, 28]. Figure 1(e) shows the reflection spectra of another thick BP sample (pink-purple region in the inset) under cross polarization with six different sample rotation angles. Here, the BP sample

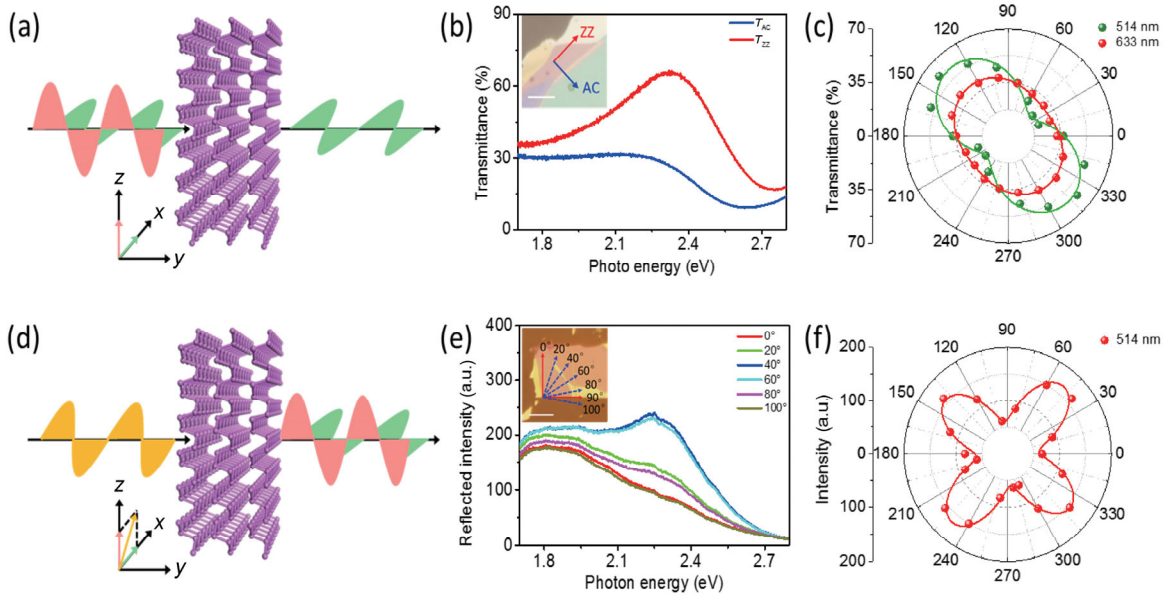

Figure 1 Linear dichroism and birefringence effect in the BP crystals. (a) and (d) Schematic illustration of the linear dichroism and birefringence effect in the BP crystals; *x* and *z* denote the zigzag (ZZ) and armchair (AC) crystal orientations, respectively. (b) Polarization dependent transmittance spectra of the BP sample (pink region) with the collection analyzer polarized along the zigzag (red line) and armchair (blue line) crystalline direction, respectively. Inset: optical image of the BP sample and the confirmed ZZ (red arrow) and AC (blue arrow) crystalline orientations, the scale bar is 10 μm. (c) Polarization-angle-dependent transmittance of the corresponding BP sample under the excitation wavelengths of 632.8 nm (red line) and 514.5 nm (green line). (e) Sample rotation angle-dependent reflection spectra of the BP sample under cross polarization. Inset: optical image of the BP sample with six rotation angles and crystal orientations shown by the blue and red arrows, respectively. The scale bar is 10 μm. (f) Polar plot of the angle-dependent reflection of the BP sample at 514.5 nm

was rotated under cross polarization, and the starting position is shown in the top left inset of Fig. 1(e). Figure 1(f) illustrates the plotted reflection intensity as a function of the sample rotation angle at 514.5 nm. This BP sample showed the largest reflection intensity at the rotation angles of 45° and 135°, while the minimum reflected intensity occurred when the incident polarization was along the crystalline axes (0° and 90°), which were identified by the corresponding angle-resolved polarized Raman results of this BP sample (Fig. S2 in the ESM). Since the reflection spectrum of the 300 nm Si/SiO_2 substrate remains constant when the BP sample is rotated under cross polarization, the angle-dependent reflection spectrum of the BP sample further confirms a significant birefringence effect in the BP crystals.

The above experiments demonstrate that the polarization of the incident light can be greatly altered by the BP layer, which can act as either absorptive optical polarizer or wave plate depending on the polarization configurations. To demonstrate that such polarization modulation can be effectively exerted on a second material, we constructed a BP-Bi_2Se_3 stacking structure, as schematically illustrated in Fig. 2(a). It was found that the polarization of the light passing through the thin BP layer and interacting with Bi_2Se_3 was different from that of the incident light on the BP surface. The BP-Bi_2Se_3 stacking structure (Fig. 2(b)) was constructed by exfoliating thin BP flakes directly on the Bi_2Se_3 crystals, which were synthesized through van der Waals epitaxy on mica substrates [35]. The AFM image in Fig. 2(d) shows that the thicknesses of the BP flake and the Bi_2Se_3 crystal below were 73 and 25 nm, respectively. As illustrated in Fig. 2(c), the Raman spectrum of the BP-Bi_2Se_3 stacking structure in the overlapped region was comprised of the Raman modes from both crystals. As it can be noted, the three modes in the lower frequency range (black) are assigned to the A_{1g}^1 (72 cm^{-1}), E_g^2 (130 cm^{-1}), and A_{1g}^2 (173 cm^{-1}) modes of Bi_2Se_3. The inset shows the corresponding atomic displacements of these modes, indicating that the two A_{1g} modes are out-of-plane

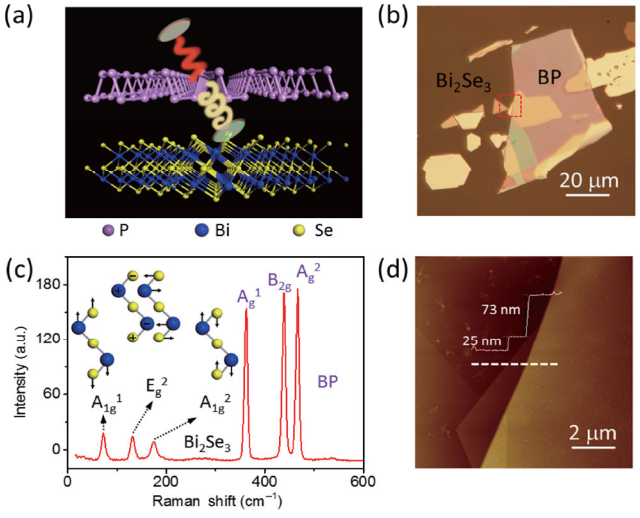

Figure 2 Concept of BP nano-optical polarization element in a BP-Bi_2Se_3 stacking structure and its characterization. (a) Schematic illustration of the BP-based nano-optical polarization element in the BP-Bi_2Se_3 stacking structure, where the polarization of the incident light interacting with Bi_2Se_3 is altered by the upper BP layer. Optical image (b), Raman characterization (c), and AFM image (d) of the BP-Bi_2Se_3 stacking structure on a mica substrate. Insets show the atomic displacements of the A_{1g}^1 (72 cm^{-1}), E_g^2 (130 cm^{-1}), and A_{1g}^2 (173 cm^{-1}) Raman modes in Bi_2Se_3. The Raman modes of Bi_2Se_3 and BP are marked in black and purple, respectively.

lattice vibrations, while the E_g mode is an in-plane lattice vibration. The other three strong Raman peaks (marked in purple) originated from the A_g^1 (362 cm^{-1}), B_{2g} (440 cm^{-1}), and A_g^2 (366 cm^{-1}) modes of BP [22, 36, 37].

Angle-resolved polarized Raman spectroscopy (ARPRS) experiments under parallel and cross polarization were performed on both the bare Bi_2Se_3 crystal and BP-Bi_2Se_3 stacking structure, respectively. The experimental setup for the measurement of the polarized Raman spectra is shown in Fig. S4 in the ESM. Figures 3(a) and 3(d) display the polarized Raman spectra of the bare Bi_2Se_3 crystal and the Bi_2Se_3 crystal with the BP layer (Fig. 2(b)) at different sample rotation angles under parallel polarization. It can be seen that the bare Bi_2Se_3 crystal exhibited three characteristic vibrational modes under parallel polarization, and their intensities did not show any obvious variation when the sample was rotated clockwise from 30° to 210°. However, for the Bi_2Se_3 crystal under the BP layer, the Raman intensities of these modes exhibited obvious angular dependent variations, which gradually decreased when the sample rotation angle changed from 30° to 120°, and then increased reaching a

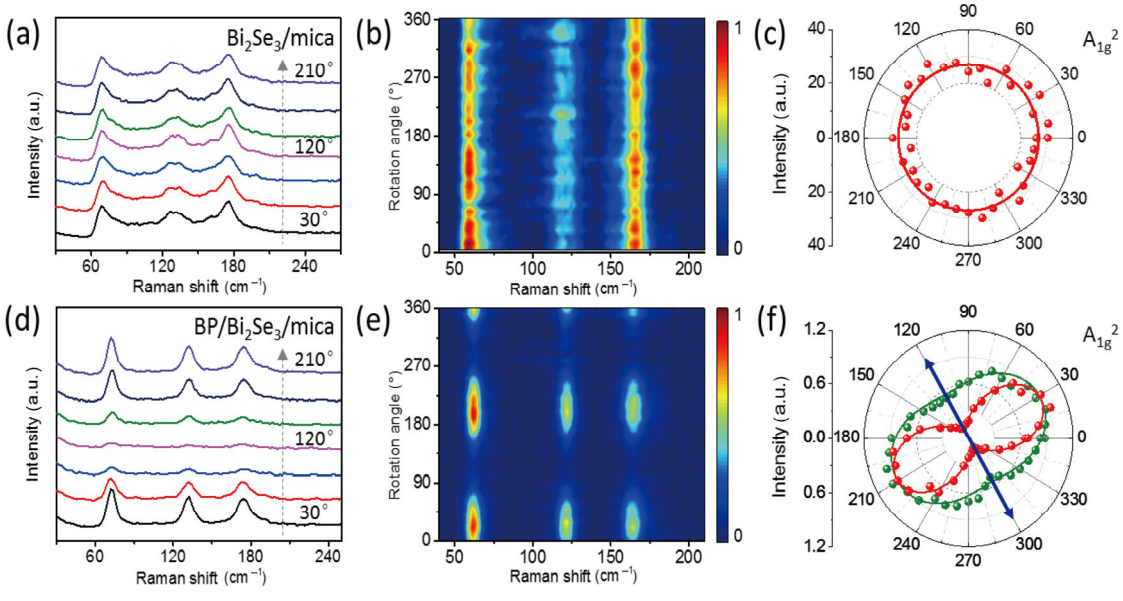

Figure 3 BP modulates the Raman spectra of the Bi_2Se_3 crystal at different rotation angles under parallel polarization. ((a) and (d)) Polarized Raman spectra of the Bi_2Se_3 crystal at different sample rotation angles without (a) or with (d) BP flakes on top. (b) and (e) Angular dependence of the normalized Raman intensity spectra for the Bi_2Se_3 crystal without (b) or with (e) BP. ((c) and (f)) Polar plots of the normalized angle-resolved polarized Raman intensities for the A_{1g}^2 mode (173 cm^{-1}) of the bare Bi_2Se_3 crystal (c) and with BP flakes (f) on top under 514.5 nm (red dots) and 632.8 nm (green dots) excitations.

maximum at 210°. Figures 3(b) and 3(e) present the angular dependence of the normalized Raman intensity spectra under parallel polarization for the bare Bi_2Se_3 crystal and the Bi_2Se_3 crystal under BP, respectively. It is evident that the Raman spectrum of the bare Bi_2Se_3 crystal did not exhibit any polarization dependence; thus, the polar plot of the intensity as a function of the rotation angle could be nicely fitted by a circle (Fig. 3(c)), by selecting the A_{1g}^2 mode as an example. This was consistent with the calculated Raman efficiency of the A_{1g} mode in the Bi_2Se_3 crystal (Section S5 in the ESM). In contrast, the Raman modes of the Bi_2Se_3 crystal under BP exhibited periodic variation features, affording two-lobed shapes with maximum (minimum) intensity angles at about 30° or 210° (120° or 300°) under both 514.5 nm (red dots) and 632.8 nm (green dots) excitation wavelengths, as illustrated in Fig. 3(f). On the other hand, the AC and ZZ crystalline orientations of the 73 nm-thick BP, which were confirmed through the angle-dependent polarized Raman intensity of the A_g modes in BP (Fig. S3 in the ESM), simply coincided with the minimum and maximum Raman intensities of the Bi_2Se_3 crystal, respectively. As discussed above, the BP sample transmits less and adsorbs more light polarized along the AC direction than that along the ZZ direction; thus, Bi_2Se_3 exhibits minimum and maximum Raman intensities. The ratio between the maximum and minimum intensities for different modes were as large as 12 at 514.5 nm (Table 1). In comparison with the results at 514.5 nm, the Raman intensity ratio was smaller at 632.8 nm, which is consistent with the relatively smaller transmittance difference of BP (green line) observed in Fig. 1(c).

The polarization state of the laser after passing through the thin BP film can be evaluated by considering the anisotropic absorption and birefringence effect in BP. As illustrated in Figs. 1(b) and 1(d), and Fig. S6 in the ESM, due to the birefringence effect in BP, the incident electric vector can be decomposed into two orthogonally polarized components $\boldsymbol{E}_x$ and $\boldsymbol{E}_z$, which propagate in BP with different velocities and attenuation coefficients, and can be expressed as

$$\boldsymbol{E}_x(y,t) = t_x E_0 \cos\theta \cos(wt - ky) \quad (1)$$

$$\boldsymbol{E}_z(y,t) = t_z E_0 \cos\theta \cos(wt - ky + \delta) \quad (2)$$

where θ is the angle between the incident polarization and AC axis of BP, δ is the induced phase difference between $\boldsymbol{E}_x$ and $\boldsymbol{E}_z$, E_0 is the initial amplitude of the incident electromagnetic wave, and t_x and t_z are the transmission coefficients of the two electric field components $\boldsymbol{E}_x$ and $\boldsymbol{E}_z$, respectively. Therefore, the outgoing light turns out to be an elliptically polarized light, which can be decomposed into the parallel and perpendicular components $\boldsymbol{e}_{i//}$ and $\boldsymbol{e}_{i\perp}$ (Fig. S6(b) in the ESM), whose intensities ($I_{//}$ and $I_\perp$) are expressed as following

$$I_{//} = T_x(E_0 \sin^2\theta)^2 + T_z(E_0 \cos^2\theta)^2 + 2(t_x E_0 \sin^2\theta) \times (t_z E_0 \cos^2\theta)\cos\delta \quad (3)$$

$$I_\perp = T_x(E_0 \sin\theta\cos\theta)^2 + T_z(E_0 \sin\theta\cos\theta)^2 + 2t_x t_z {E_0}^2 \sin^2\theta\cos^2\theta\cos\delta \quad (4)$$

where T_x ($T_x = t_x^2$) and T_z ($T_z = t_z^2$) are the transmittance of the polarized light along the ZZ and AC axes of the BP crystal. According to the Raman selection rule, the A_{1g} modes of the Bi_2Se_3 crystal are allowed under parallel polarization, while being forbidden under cross polarization, as shown in Section S5 in the ESM (Table S1 in the ESM). As a consequence, the parallel ($\boldsymbol{e}_{i//}$) and perpendicular ($\boldsymbol{e}_{i\perp}$) components contribute to the polarized Raman signals of the A_{1g} modes in the Bi_2Se_3 crystal under parallel and cross polarizations, respectively. We further calculated the Raman efficiency of the A_{1g} modes in the Bi_2Se_3 crystal with a BP layer, by considering the anisotropic absorption and birefringence effect under parallel ($S_{A_{1g}//}$) and cross ($S_{A_{1g}\perp}$) polarizations (Section S6 in the ESM), expressed as

$$S_{A_{1g}//} = a^2 {t_x}^4 \sin^4\theta + 2a^2 {t_x}^2 {t_z}^2 \sin^2\theta\cos^2\theta\cos 2\delta + a^2 {t_z}^4 \cos^4\theta \quad (5)$$

$$S_{A_{1g}\perp} = a^2 \sin^2\theta\cos^2\theta({t_x}^4 - 2{t_x}^2{t_z}^2\cos 2\delta + {t_z}^4) \quad (6)$$

Table 1 Maximum and minimum intensity ratio (I_{ZZ}/I_{AC}) of the different Raman modes of Bi_2Se_3 under parallel polarization at 514.5 and 632.8 nm excitation wavelengths

Wavelength (nm)	A_{1g}^1	E_g^2	A_{1g}^2
514.5	12.8	13.2	7.8
632.8	—	1.8	1.9

where a is the Raman tensor element of the A_{1g} modes in Bi_2Se_3. It can be seen from Eq. (5) that the birefringence of BP has a little effect on the Raman intensity of the Bi_2Se_3 crystal under parallel polarization, since the value of the polynomial containing the birefringence induced phase difference is either negligible or even zero when the incident polarization is parallel to the ZZ and AC lattice directions of BP (Eq. (3)). In addition, the fitted transmittance ratio (T_x/T_z) for the 73 nm-thick BP according to the Raman intensities of Bi_2Se_3 under parallel polarization is in good agreement with the measured results for the BP sample (65 nm) with roughly equal thickness, under both 514.5 and 632.8 nm excitations (Figs. 1(b) and 1(c), Tables S2 and S3 in the ESM). The polarization modulation ability of BP as a linear polarizer was also further confirmed by the measurements of the photoluminescence (PL) and Raman scattering signals of a monolayer WS_2 in a BP-WS_2 stacking structure (Fig. S5 in the ESM). Besides the Raman intensity, the PL emission of the monolayer WS_2 also showed a maximum and minimum intensity when the incident light was polarized along the ZZ and AC axes of BP, respectively.

Since the light passing through BP contains a polarization component perpendicular to that of the incident light, which should contribute to the Raman signals of the Bi_2Se_3 crystal under cross polarization, we further measured the polarized Raman spectra of the Bi_2Se_3 crystal in the stacking region under cross polarization. Figures 4(a) and 4(d) show the polarized Raman spectra of the bare Bi_2Se_3 crystal and Bi_2Se_3 crystal with BP (Fig. 2(b)) at different sample rotation angles, respectively. As presented in Figs. 4(a) and 4(b), only one Raman peak (E_g^2 mode) appeared in the Raman spectra of the bare Bi_2Se_3 crystal under cross polarization, and its intensity remained unchanged upon variation of the rotation angle. The intensity polar plot of the E_g^2 mode of the bare Bi_2Se_3 crystal still displayed a circular shape, demonstrating that this mode did not exhibit a polarization dependence under cross polarization (Fig. 4(c)), in accordance with the calculated Raman efficiency trend based on the group theory (Section S5 in the ESM). Interestingly, in the presence of the thin BP layer on top, all three Raman modes appeared in the Raman spectra of the Bi_2Se_3 crystal. On the other hand, the A_{1g}^1 and A_{1g}^2 modes, which should be silent under cross polarization

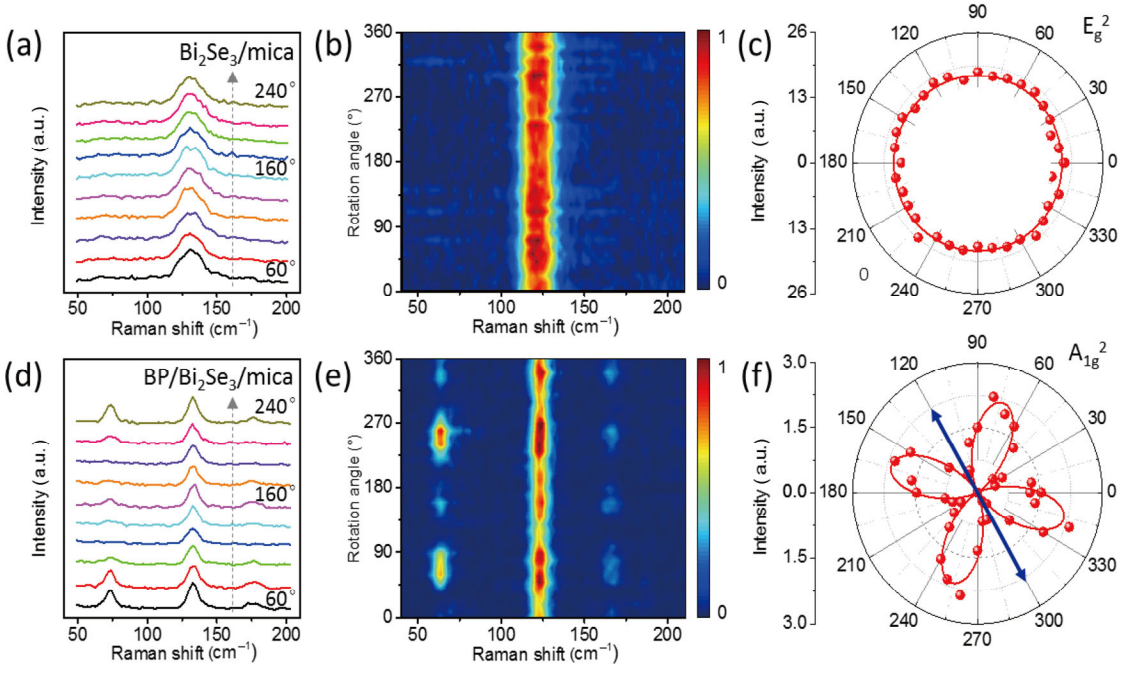

Figure 4 Raman spectra of the Bi_2Se_3 crystal at different rotation angles under cross polarization at 514.5 nm. Polarized Raman spectra of the Bi_2Se_3 crystal at different sample rotation angles without (a) or with (d) BP flakes on top. Angular dependence of the normalized Raman intensity spectra for the Bi_2Se_3 crystal without (b) or with (e) BP. Polar plots of the angle-resolved polarized Raman intensities for the E_g^2 mode (130 cm^{-1}) of the Bi_2Se_3 crystal without BP flake (c) and the A_{1g}^2 (173 cm^{-1}) mode (f) with BP flakes.

according to the Raman selection rule, not only emerged in the Raman spectra, but also showed an obvious polarization dependent behavior. Figure 4(e) shows the angular dependences of the normalized Raman intensity spectra in the cross-polarized configuration. It can be clearly seen that in the presence of BP on top, the A_{1g} modes of the Bi_2Se_3 crystal yielded a four-lobed shape with four maximum intensity angles at 75°, 165°, 255°, and 345°, which happened to be 45° relative to the crystal axes of the BP crystals. This phenomenon was also consistent with the calculated Raman scattering efficiency of the A_{1g} modes in the Bi_2Se_3 crystal with a BP layer in Eq. (6), which is $a^2 \sin^2\theta\cos^2\theta(t_x{}^4 - 2t_x{}^2t_z{}^2\cos 2\delta + t_z{}^4)$. Meanwhile, as indicated in Eqs. (4) and (6), the emergence of the A_{1g}^1 and A_{1g}^2 modes under cross polarization can be attributed to the perpendicular component induced by the combined effect of the birefringence (δ) and linear dichroism of BP, which is parallel to the polarization of the analyzer. We calculated the Raman scattering efficiency of the Bi_2Se_3 crystal with BP under cross polarization by considering either only the anisotropic absorption or the birefringence. The contribution of the anisotropic absorption $a^2 \sin^2\theta\cos^2\theta(t_x{}^4 - t_z{}^4)$, was much weaker under cross polarization than that of the birefringence effect $a^2 \sin^2\theta\cos^2\theta(t_x{}^4 - 2\cos 2\delta)$ (Fig. S7 in the ESM). Here, t_x^2 and t_z^2 refer to the measured anisotropic transmittance of the polarized light along the ZZ and AC directions of the 73 nm-thick BP at 514.5 nm, t_x^2 = 0.60, t_z^2 = 0.21. The phase difference δ can be obtained by fitting the polarized Raman intensities of the A_{1g} modes in Bi_2Se_3 under parallel polarization (Table S2 and Section S6 in the ESM). In this regard, the above experiments demonstrated that the 73 nm-thick BP behaved as a wave plate to modulate the Raman signals of the Bi_2Se_3 crystal under cross polarization. On the contrary, the in-plane vibrational E_g^2 mode of the bare Bi_2Se_3 crystal, which is not sensitive to the rotation of the incident polarization in the x–z plane according to the Raman selection rule, displayed the same intensity under both cross and parallel polarization, thus its intensity did not show such an obvious dependence on the sample rotation as the A_{1g} mode (Fig. S8 in the ESM).

4 Conclusions

In view of the 2D structure and robust in-plane optical anisotropy of BP, we designed a BP-Bi_2Se_3 stacking structure, whose thin BP layer was demonstrated to alter the polarization of the incident laser, resulting in an exceptional angular dependence of the Raman scattering of the Bi_2Se_3 crystal under both parallel and cross polarization. Specifically, the 73 nm thick-BP layer behaved as a linear polarizer under parallel polarization; the intensities of all the Raman modes of Bi_2Se_3 exhibited a maximum and minimum with the incident polarization along the ZZ and AC directions of BP, respectively. Furthermore, the intensity ratio between the maxima and minima was as high as 12 at 514.5 nm. Besides, under cross polarization, the A_{1g} modes of the Bi_2Se_3 crystal, which should have been silent , not only appeared in the Raman spectra of the BP-Bi_2Se_3 stacking structure, but also showed a clear polarization-angle dependence. This was attributed to the birefringence effect of BP, which leads to a polarization component perpendicular to that of the incident laser. Although certain limitations exist, such as the stability of BP and a decreased transmittance upon increasing thickness, the results of this study suggest a promising way to design novel optical polarization elements with nanoscale thickness based on 2D anisotropic crystals, which can be directly integrated in photonic and optoelectronic devices for polarization modulation.

Acknowledgements

J. Z. and L. M. T. acknowledge the funding from the National Natural Science Foundation of China (NSFC) (Nos. 21233001, 51272006, 11374355, and 21573004) and the National Basic Research Program of China (Nos. 2016YFA0200101, 2016YFA0200104, and 2015CB932400). H. X. acknowledges the funding of the National Natural Science Foundation of China (No. 51502167). The authors thank X. L. for the constructive discussion.

Electronic Supplementary Material: Supplementary material (further details of experimental setup, the angle-dependent polarized Raman of the BP sample,

PL and Raman spectra of WS_2 in the stacking structure, Raman selection rule of Bi_2Se_3 crystal with BP on the top) is available in the online version of this article at https://doi.org/10.1007/s12274-017-1690-4.

References

[1] Sun, Z. P.; Martinez, A.; Wang, F. Optical modulators with 2D layered materials. *Nat. Photonics* **2016**, *10*, 227–238.

[2] Reed, G. T.; Mashanovich, G.; Gardes, F. Y.; Thomson, D. J. Silicon optical modulators. *Nat. Photonics* **2010**, *4*, 518–526.

[3] Fang, Y. R.; Sun, M. T. Nanoplasmonic waveguides: Towards applications in integrated nanophotonic circuits. *Light: Sci. Appl.* **2015**, *4*, e294.

[4] Xia, F. N.; Wang, H.; Xiao, D.; Dubey, M.; Ramasubramaniam, A. Two-dimensional material nanophotonics. *Nat. Photonics* **2014**, *8*, 899–907.

[5] Chen, R.; Ng, K. W.; Ko, W. S.; Parekh, D.; Lu, F. L.; Tran, T.-T. D.; Li, K.; Chang-Hasnain, C. Nanophotonic integrated circuits from nanoresonators grown on silicon. *Nat. Commun.* **2014**, *5*, 4325.

[6] Zhao, Y.; Belkin, M. A.; Alù, A. Twisted optical metamaterials for planarized ultrathin broadband circular polarizers. *Nat. Commun.* **2012**, *3*, 870.

[7] Arbabi, A.; Horie, Y.; Bagheri, M.; Faraon, A. Dielectric metasurfaces for complete control of phase and polarization with subwavelength spatial resolution and high transmission. *Nat. Nanotechnol.* **2015**, *10*, 937–943.

[8] Liu, F. C.; Zheng, S. J.; He, X. X.; Chaturvedi, A.; He, J. F.; Chow, W. L.; Mion, T. R.; Wang, X. L.; Zhou, J. D.; Fu, Q. D. et al. Highly sensitive detection of polarized light using anisotropic 2D ReS_2. *Adv. Funct. Mater.* **2015**, *26*, 1169–1177.

[9] Bao, Q. L.; Zhang, H.; Wang, B.; Ni, Z. H.; Lim, C. H. Y. X.; Wang, Y.; Tang, D. Y.; Loh, K. P. Broadband graphene polarizer. *Nat. Photonics* **2011**, *5*, 411–415.

[10] Tan, Y.; He, R. Y.; Cheng, C.; Wang, D.; Chen, Y. X.; Chen, F. Polarization-dependent optical absorption of MoS_2 for refractive index sensing. *Sci. Rep.* **2014**, *4*, 7523

[11] De Oliveira, R. E. P.; De Matos, C. J. S. Graphene based waveguide polarizers: In-depth physical analysis and relevant parameters. *Sci. Rep.* **2015**, *5*, 16949.

[12] Yang, J.; Wang, Z.; Wang, F.; Xu, R. J.; Tao, J.; Zhang, S.; Qin, Q. H.; Luther-Davies, B.; Jagadish, C.; Yu, Z. F. et al. Atomically thin optical lenses and gratings. *Light: Sci. Appl.* **2016**, *5*, e16046.

[13] Grande, M.; Bianco, G. V.; Vincenti, M. A.; De Ceglia, D.; Capezzuto, P.; Scalora, M.; D'Orazio, A.; Bruno, G. Optically transparent microwave polarizer based on quasi-metallic graphene. *Sci. Rep.* **2015**, *5*, 17083.

[14] Qiao, J. S.; Kong, X. H.; Hu, Z.-X.; Yang, F.; Ji, W. High-mobility transport anisotropy and linear dichroism in few-layer black phosphorus. *Nat. Commun.* **2014**, *5*, 4475.

[15] Xia, F. N.; Wang, H.; Jia, Y. C. Rediscovering black phosphorus as an anisotropic layered material for optoelectronics and electronics. *Nat. Commun.* **2014**, *5*, 4458.

[16] Li, L. K.; Yu, Y. J.; Ye, G. J.; Ge, Q. Q.; Ou, X. D.; Wu, H.; Feng, D. L.; Chen, X. H.; Zhang, Y. B. Black phosphorus field-effect transistors. *Nat. Nanotechnol.* **2014**, *9*, 372–377.

[17] Zhang, S.; Yang, J.; Xu, R. J.; Wang, F.; Li, W. F.; Ghufran, M.; Zhang, Y.-W.; Yu, Z. F.; Zhang, G.; Qin, Q. H. et al. Extraordinary photoluminescence and strong temperature/angle-dependent Raman responses in few-layer phosphorene. *ACS Nano* **2014**, *8*, 9590–9596.

[18] Li, L. K.; Kim, J.; Jin, C. H.; Ye, G. J.; Qiu, D. Y.; da Jornada, F. H.; Shi, Z. W.; Chen, L.; Zhang, Z. C.; Yang, F. Y. et al. Direct observation of the layer-dependent electronic structure in phosphorene. *Nat. Nanotechnol.* **2017**, *12*, 21–25.

[19] Lan, S. F.; Rodrigues, S.; Kang, L.; Cai, W. S. Visualizing optical phase anisotropy in black phosphorus. *ACS Photonics* **2016**, *3*, 1176–1181.

[20] Wang, X. M.; Jones, A. M.; Seyler, K. L.; Tran, V.; Jia, Y. C.; Zhao, H.; Wang, H. W.; Yang, L.; Xu, X. D.; Xia, F. N. Highly anisotropic and robust excitons in monolayer black phosphorus. *Nat. Nanotechnol.* **2015**, *10*, 517–521.

[21] Ling, X.; Huang, S. X.; Hasdeo, E. H.; Liang, L. B.; Parkin, W. M.; Tatsumi, Y.; Nugraha, A. R. T.; Puretzky, A. A.; Das, P. M.; Sumpter, B. G. et al. Anisotropic electron-photon and electron-phonon interactions in black phosphorus. *Nano Lett.* **2016**, *16*, 2260–2267.

[22] Wu, J. X.; Mao, N. N.; Xie, L. M.; Xu, H.; Zhang, J. Identifying the crystalline orientation of black phosphorus using angle-resolved polarized Raman spectroscopy. *Angew. Chem., Int. Ed.* **2015**, *54*, 2366–2369.

[23] Mao, N. N.; Wu, J. X.; Han, B. X.; Lin, J. J.; Tong, L. M.; Zhang, J. Birefringence-directed Raman selection rules in 2D black phosphorus crystals. *Small* **2016**, *12*, 2627–2633.

[24] Mao, N. N.; Tang, J. Y.; Xie, L. M.; Wu, J. X.; Han, B. W.; Lin, J. J.; Deng, S. B.; Ji, W.; Xu, H.; Liu, K. H. et al. Optical anisotropy of black phosphorus in the visible regime. *J. Am. Chem. Soc.* **2016**, *138*, 300–305.

[25] Ribeiro, H. B.; Villegas, C. E. P.; Bahamon, D. A.; Muraca, D.; Neto, A. H. C.; de Souza, E. A. T.; Rocha, A. R.; Pimenta, M. A.; de Matos, C. J. S. Edge phonons in black phosphorus. *Nat. Commun.* **2016**, *7*, 12191.

[26] Ribeiro, H. B.; Pimenta, M. A.; de Matos, C. J. S.; Moreira, R. L.; Rodin, A. S.; Zapata, J. D.; de Souza, E. A. T.; Neto, A. H. C. Unusual angular dependence of the Raman response in black phosphorus. *ACS Nano* **2015**, *9*, 4270–4276.

[27] Tran, V.; Soklaski, R.; Liang, Y. F.; Yang, L. Layer-controlled band gap and anisotropic excitons in few-layer black phosphorus. *Phys*. *Rev*. *B* **2014**, *89*, 235319.

[28] Kim, J.; Lee, J. U.; Lee, J.; Park, H. J.; Lee, Z.; Lee, C.; Cheong, H. Anomalous polarization dependence of Raman scattering and crystallographic orientation of black phosphorus. *Nanoscale* **2015**, *7*, 18708–18715.

[29] Lu, J. P.; Yang, J.; Carvalho, A.; Liu, H. W.; Lu, Y. R.; Sow, C. H. Light-matter interactions in phosphorene. *Acc*. *Chem*. *Res*. **2016**, *49*, 1806–1815.

[30] Zhang, G. W.; Huang, S. Y.; Chaves, A.; Song, C. Y.; Özçelik, V. O.; Low, T.; Yan, H. G. Infrared fingerprints of few-layer black phosphorus. *Nat*. *Commun*. **2017**, *8*, 14071.

[31] Hong, T.; Chamlagain, B.; Wang, T. J.; Chuang, H.-J.; Zhou, Z. X.; Xu, Y.-Q. Anisotropic photocurrent response at black phosphorus-MoS_2 p-n heterojunctions. *Nanoscale* **2015**, *7*, 18537–18541.

[32] Hong, T.; Chamlagain, B.; Lin, W. Z.; Chuang, H.-J.; Pan, M. H.; Zhou, Z. X.; Xu, Y.-Q. Polarized photocurrent response in black phosphorus field-effect transistors. *Nanoscale* **2014**, *6*, 8978–8983.

[33] Yuan, H. T.; Liu, X. G.; Afshinmanesh, F.; Li, W.; Xu, G.; Sun, J.; Lian, B.; Curto, A. G.; Ye, G. J.; Hikita, Y. et al. Polarization-sensitive broadband photodetector using a black phosphorus vertical p–n junction. *Nat*. *Nanotechnol*. **2015**, *10*, 707–713.

[34] Wang, G. C.; Bao, L. H.; Pei, T. F.; Ma, R. S.; Zhang, Y.-Y.; Sun, L. L.; Zhang, G. Y.; Yang, H. F.; Li, J. J.; Gu, C. Z. et al. Introduction of interfacial charges to black phosphorus for a family of planar devices. *Nano Lett*. **2016**, *16*, 6870–6878.

[35] Peng, H. L.; Dang, W. H.; Cao, J.; Chen, Y. L.; Wu, D.; Zheng, W. S.; Li, H.; Shen, Z.-X.; Liu, Z. F. Topological insulator nanostructures for near-infrared transparent flexible electrodes. *Nat*. *Chem*. **2012**, *4*, 281–286.

[36] Sugai, S.; Ueda, T.; Murase, K. Pressure dependence of the lattice vibration in the orthorhombic and rhombohedral structures of black phosphorus. *J*. *Phys*. *Soc*. *Jpn*. **1981**, *50*, 3356–3361.

[37] Ling, X.; Liang, L. B.; Huang, S. X.; Puretzky, A. A.; Geohegan, D. B.; Sumpter, B. G.; Kong, J.; Meunier, V.; Dresselhaus, M. S. Low-frequency interlayer breathing modes in few-layer black phosphorus. *Nano Lett*. **2015**, *15*, 4080–4088.